

基于玻尔兹曼图法的超燃冲压发动机 温度测量方法研究

黄安^{1,2}, 赵延辉³, 杨顺华³, 夏晖晖¹, 邓昊¹, 阮俊¹, 胡佳屹¹, 艾苏曼¹, 许振宇^{1*}, 阚瑞峰^{1**}

¹中国科学院合肥物质科学研究院安徽光学精密机械研究所, 安徽 合肥 230031;

²中国科学技术大学研究生院科学岛分院, 安徽 合肥 230026;

³中国空气动力研究与发展中心超高速空气动力研究所, 四川 绵阳 621000

摘要 为提高超燃冲压发动机扩张段温度测量精度和测量结果的稳定性,笔者基于可调谐半导体吸收光谱技术(TDLAS),选取5个低态能级不同且分布均匀的近红外H₂O吸收线,采用玻尔兹曼图法测温。采用集成的五波长测量系统,在实验室高温炉上设定1000~1600 K的温度台阶,选用不同波长数目组合计算分析,五波长的温度偏差均在1%之内,优于其他数目的波长组合。在发动机实验中,测量了超燃冲压发动机扩张段横截面16路线的平均温度,实现了发动机点火、燃烧和熄火宽温度范围的监测;对比了相同工况下的两次实验,结果显示,工况A和工况B下重复实验的平均偏差分别为17 K和7 K,重复性较好,体现该测量方法在发动机测量中的稳定性。该温度测量方法可广泛应用于发动机及工业过程的燃烧流场领域,为计算燃烧效率、改进燃烧过程提供数据支撑,具有重要的工程应用价值。

关键词 光谱学; 可调谐半导体吸收光谱技术; 玻尔兹曼图; 温度测量

中图分类号 O433.1

文献标志码 A

DOI: 10.3788/CJL221338

1 引言

基于可调谐半导体吸收光谱(TDLAS)技术的温度测量技术已被广泛应用于工业锅炉、超燃冲压发动机、燃气轮机以及航空发动机等燃烧器^[1-3]燃烧流场的测量。单光路TDLAS测温方法按所选吸收谱线的数目可分为单线测温法、双线测温法、多线测温法^[4]。单线测温法利用多普勒展宽与温度的单调关系精确测量多普勒展宽,从而反演出温度,适用于多普勒展宽远大于碰撞展宽的条件下,在燃烧电弧风洞等一类超高温低压环境中的应用较多^[5]。双线测温法选取同一气体分子不同低态能级的两条吸收线,利用它们线强比值与温度单调变化的关系计算出温度。为适应不同温度段的测量,提高测温灵敏度,通常选取低态能级差大的吸收线组^[6]进行双线测温。但低态能级差较大的吸收线组往往线强较为悬殊,而且实际的恶劣燃烧环境会导致吸收信号的信噪比较差,同时,光束抖动、气流密度不均匀、火焰背景辐射等带来的非吸收传输损耗也会影响测量精度^[7]。此外,双线计算需要引用HITEMP或HITRAN光谱数据库中的线强参数,较

大的不确定度会影响计算精度。利用免标定波长调制技术反演时,还会用到自展宽、空气展宽及温度依赖系数进行建模,而在实际的燃烧环境中,气体间碰撞的分子不局限于空气中的分子,导致引用数据库中的参数会增大误差^[8]。多线测温选取一系列低态能级不同的吸收线,通过增加波长的数目来增大该方法的抗噪能力,从而提高了测量精度。在实际的发动机应用中,点火、燃烧、熄火阶段的温度范围跨度较大,多波长方案可对全程进行监测,为测量提供更全面的信息^[9]。在解决这类问题时,多线测温法相较于双线测温法具有一定优势。

多线测温法可分为两大类,其中一类是利用连续扫描的宽波段对整个光谱进行处理分析,获得温度、浓度及其他信息。Wang等^[10]利用宽带光源扫描了1335~1375 nm范围内的吸收谱线并实现了300~2000 K温度、0.1~2.5 MPa压力范围内燃烧室二维温度组分场分布的重建;艾苏曼等^[11]模拟分析了不同类型误差下7361.476~7485.0797 cm⁻¹范围内宽波段测温的精度。受激光器出光不稳定的影响,宽波段扫描中的基线往往是不规则的,从而增大了吸光度信号提

收稿日期: 2022-10-18; 修回日期: 2022-11-18; 录用日期: 2022-11-30; 网络首发日期: 2022-12-10

基金项目: 国家重点研发计划(2020YFA0405703, 2019YFB2006003)、国家自然科学基金(618052986)、安徽省自然科学基金(2008085QF317)

通信作者: *zyxu@aiofm.ac.cn; **kanruifeng@aiofm.ac.cn

取和温度计算的误差。为了解决基线提取不准确的问题,司赶上等^[12]利用形态学和多项式拟合算法对背景基线进行校正,获得了更准确的吸光度信号。另一类多线测温法选择独立不连续的吸收线,利用低态能级与积分吸光度之间的线性关系进行求解,即玻尔兹曼图法。例如,Busa等^[13]采用3支分布式反馈(DFB)激光器覆盖H₂O的6条吸收谱线,结合玻尔兹曼图法,在RC-22超燃冲压发动机上实现1 kHz的温度测量。玻尔兹曼图法测温可利用多支DFB激光器组合实现,相较于宽带光源测量方法在吸光度信号提取上更具优势,在波长选择利用上更高效,成本更低廉,系统集成更简单,更易于实现工程化。

笔者以H₂O为目标分子,选择5个低态能级分布较宽的波长,集成了一套多波长测量系统,并采用该系统分别在高温炉和直连式脉冲燃烧风洞设备上进行实

验,研究了不同波长组合玻尔兹曼图法测温的精度,评估了该测量方法在实际发动机燃烧流场诊断中的稳定性。

2 基本原理

气体的吸收遵循Beer-Lambert定律^[14],穿过待测燃烧流场的激光光强 $I(\nu)$ 可描述为

$$I(\nu) = I_0(\nu) \exp \left[- \int_0^L PXS(T)\phi(\nu)dx \right], \quad (1)$$

式中: $I_0(\nu)$ 为入射光强; P 为待测环境压强,单位为atm(1 atm=101325 Pa); X 为气体分子的物质的量分数; $S(T)$ 为分子吸收线线强,单位为 $\text{cm}^{-2}\cdot\text{atm}^{-1}$; L 为吸收路径长度,单位为cm; $\phi(\nu)$ 为归一化吸收线型函数。吸收线线强 $S(T)$ 与温度 T 之间的关系可利用温度 T_0 (T_0 一般取296 K)下的线强作参考,表示为

$$S(T) = S(T_0) \frac{Q(T_0)}{Q(T)} \left(\frac{T_0}{T} \right) \exp \left[- \frac{hcE''}{k} \left(\frac{1}{T} - \frac{1}{T_0} \right) \right] \frac{1 - \exp \left(- \frac{hc\nu_0}{kT} \right)}{1 - \exp \left(- \frac{hc\nu_0}{kT_0} \right)}, \quad (2)$$

式中: h 为普朗克常数,单位为 $\text{J}\cdot\text{s}$; c 为光速,单位为 $\text{cm}\cdot\text{s}^{-1}$; k 为玻尔兹曼常数,单位为 $\text{J}\cdot\text{K}^{-1}$; E'' 为低态能级,单位为 cm^{-1} ; $Q(T)$ 为分子内配分函数; ν_0 为吸收谱线的中心波数,单位为 cm^{-1} 。

根据式(1),吸光度信号 α_ν 可描述为

$$\alpha_\nu = - \ln \frac{I(\nu)}{I_0(\nu)} = \int_0^L PXS(T)\phi(\nu)dx = A \cdot \phi, \quad (3)$$

式中: A 为积分吸光度值。多线测温利用玻尔兹曼分布的曲线^[15],该曲线的数学表达式为

$$\ln \left[\frac{A}{S(T_0)} \right] = - \frac{hc}{k} \left(\frac{1}{T} - \frac{1}{T_0} \right) E'' + \ln(PXL) + \ln \left[\frac{Q(T_0)T_0}{Q(T)T} \right] + \ln \left[\frac{1 - \exp \left(- \frac{hc\nu_0}{kT} \right)}{1 - \exp \left(- \frac{hc\nu_0}{kT_0} \right)} \right]. \quad (4)$$

拟合不同低态能级与 $\ln[A/S(T_0)]$ 的一次多项式,斜率包含温度信息,截距包含浓度信息。对于均匀流场,所有的点均在拟合的直线上;而对于非均匀燃烧场,点会偏离拟合的直线,偏离程度会随温度梯度的增大而加剧,此时求得的价值为路径平均结果。

3 谱线选择

以燃烧流场的主要产物H₂O为目标分子,在HITEMP2010数据库中选择5条吸收谱线。选线的原则是吸收谱线低态能级覆盖范围较宽,两两间距较大,邻近位置无其他气体吸收干扰并且高温下的信噪比高^[16]。参考超燃冲压发动机的典型燃烧环境,模拟了5条吸收线在温度为1500 K、水汽的体积分数为10%、压力为50 kPa、光程为10 cm条件下的吸光度曲线,同时在H₂O的吸收上叠加了20%CO₂和10%CO的干扰。图1表明所选谱线不受干扰吸收的影响,符合选

线要求。

采用玻尔兹曼图法计算温度时需要用到HITEMP2010数据库中吸收谱线在296 K下的参考线强 S_0 和低态能级 E'' 。数据库中5条吸收谱线线强的不确定度只有7467.77 cm^{-1} 在5%~10%之间,其余均在10%~20%之间。线强误差较大会影响温度的计算精度,因此在实验室内对所选谱线的线强进行了高温标定,标定方法及不确定计算方法参考了陈玖英等^[17]发表的关于光谱参数标定的论文,标定所用高温炉平台与该论文中的一致。限于篇幅,本文不对标定过程过多描述,表1给出所选谱线中心波数、低态能级、标定后296 K下的参考线强及不确定度。为计算方便,对7444.352 cm^{-1} 和7444.369 cm^{-1} 这两条低态能级不同但波长相近的吸收线作合并处理,低态能级取两者的平均值,其余低态能级相同的相邻吸收线均作合并处理。

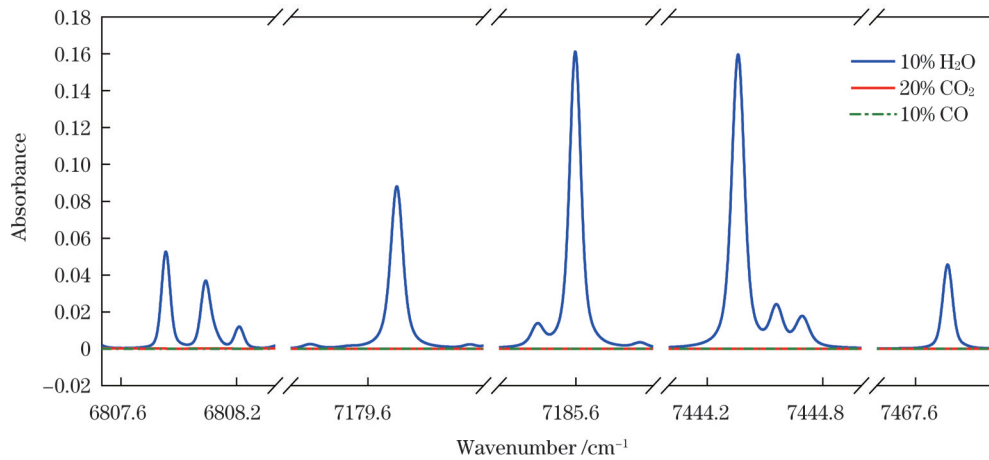


图1 所选吸收线模拟的吸光度信号

Fig. 1 Absorbance signals simulated by the selected absorption line

表1 所选谱线参数

Table 1 Selected spectral line parameters

ν / cm^{-1}	E'' / cm^{-1}	$S_0 @ \text{HITEMP2010} / (\text{cm}^{-2} \cdot \text{atm}^{-1})$	Uncertainty for $S_0 @ \text{HITEMP2010}$	Measured $S_0 / (\text{cm}^{-2} \cdot \text{atm}^{-1})$	Uncertainty for measured S_0
7467.77	2551.48	1.27×10^{-5}	5%–10%	1.09×10^{-5}	<5%
7444.352, 7444.369	1774.75, 1806.67	5.4×10^{-4} , 5.76×10^{-4}	10%–20%	1.10×10^{-3}	<5%
7179.75	1216.19	5.97×10^{-3}	10%–20%	5.81×10^{-3}	<5%
7185.597	1045.06	1.98×10^{-2}	10%–20%	1.91×10^{-2}	<5%
6807.83	3319.45	6.17×10^{-7}	10%–20%	6.03×10^{-7}	<5%

4 实验与分析

4.1 高温炉实验

在实验室内利用高温炉平台开展实验,对玻尔兹曼图法测温进行验证。图2所示为高温炉玻尔兹曼图法测温的整体方案。高温炉(MTI, GSL-1800X-III)采用三段式加热,中间恒温吸收区域长300 mm,额定最高温度为2073 K,控温精度为 ± 1 K。实验室内集成了多波长测量TDLAS系统,选用5支DFB激光器(NEL),其中心波长分别为1339、1343、1392、1393、1469 nm,另外还集成了激光器控制、分时扫描、信号发生、光纤合束模块(自研)。信号探测系统集成了光耦探测器及前置放大电路(自研)。

在集成的多波长TDLAS系统中,5组温控和信号发生模块分别控制5支激光器分时出光,产生锯齿波扫描,覆盖所选吸收谱线;单支激光器的扫描频率为20 kHz,整个系统的扫描频率为4 kHz,时间分辨为0.25 ms。1339 nm与1343 nm激光器的输出激光通过保偏合束器1(PBS1)合束,1392 nm与1393 nm激光器的输出激光通过保偏合束器2(PBS2)合束,之后再与1469 nm激光经波分复用器(WDM)合束后出光。输出的激光分成两束,其中的50%光经准直后穿过高温炉恒温区,剩下的50%光经准直后穿过标准具,分别

被准直透镜收集,经多模光纤传输至信号探测系统,由光耦探测器(Thorlabs, FGA01FC)探测后被前置放大电路放大,接入采集卡(NI, PCI5105)。在发射端、接收端准直与两端窗片之间,利用氮气吹扫来降低空气中的水汽给测量带来的干扰。

实验设定1000~1600 K范围内的7个温度台阶,在每个温度台阶下充入一定压力的纯水汽,恒温维持40 min,待温度、压力稳定后,利用集成的多波长系统进行测量。炉膛内的压力由压力计(PFEIFFER, CMR361)监测。采用玻尔兹曼图法反演每个温度台阶下的温度,并将其与设定值进行对比。实验中测得了高温炉中水汽的吸收信号以及标准具的干涉信号,如图3所示。每支激光器有一段不出光的部分,用来监测火焰辐射导致的信号整体抬高,处理数据时作为背景扣除。

每个温度台阶采集100组数据。在数据处理过程中,先对干涉信号进行时域到频域的转换,然后选取吸收信号两端无吸收区域通过三次多项式拟合 I_0 ,再根据式(3)获得吸光度信号,接着采用Voigt线型通过LM算法拟合吸光度曲线,获得各波长对应的积分吸光度值 A 。拟合5组低态能级与 $\ln[A/S(T_0)]$ 的线性关系,可获得图4所示的玻尔兹曼图,图中给出了双波长、三波长、四波长、五波长的测量值和拟合

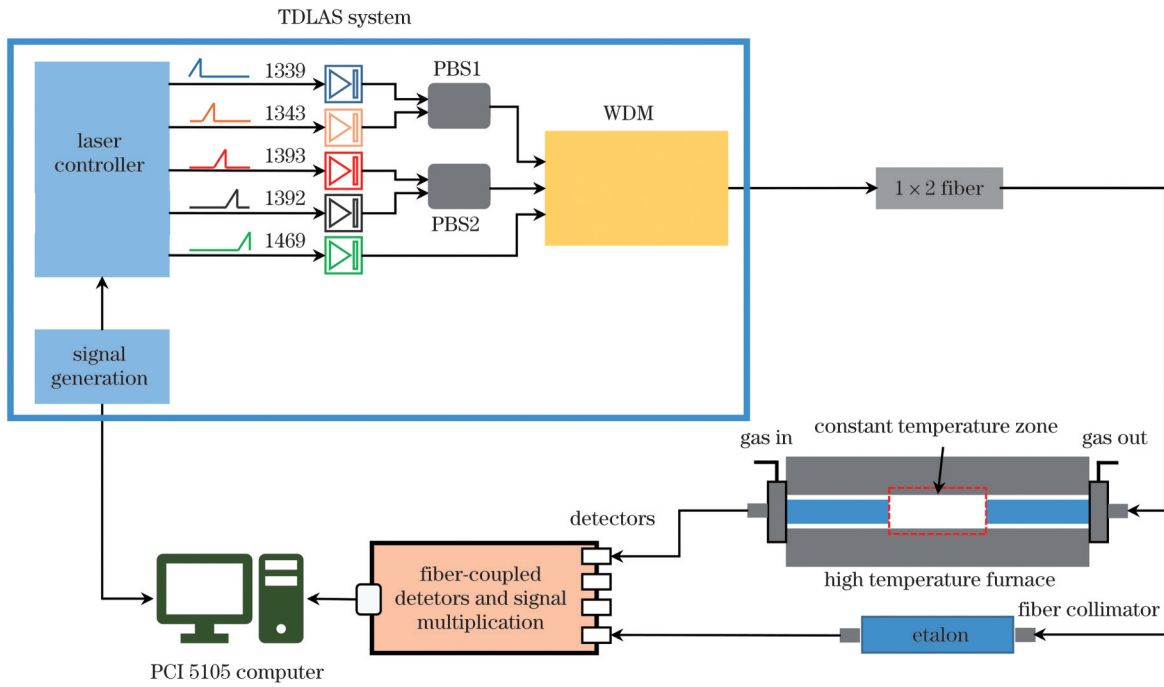


图 2 高温炉测量系统方案

Fig. 2 High-temperature furnace measurement solution

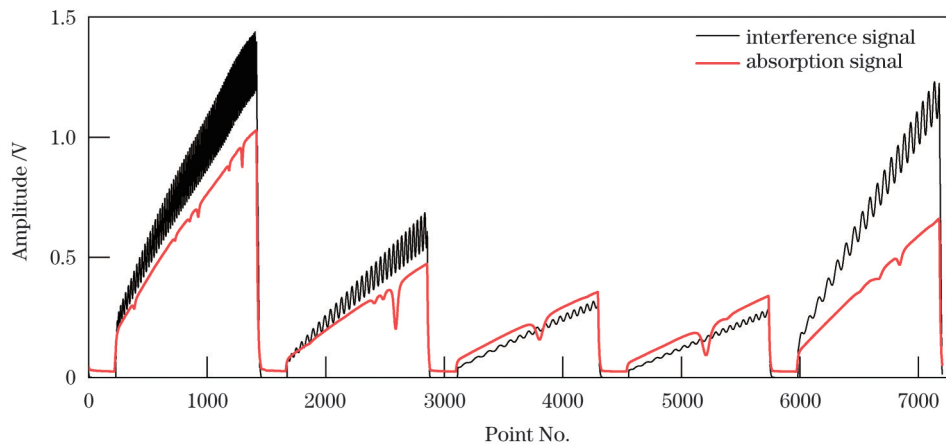


图 3 高温炉中水汽的吸收信号以及标准具的干涉信号

Fig. 3 Absorption signal of water vapor in the high-temperature furnace and interference signal of the etalon

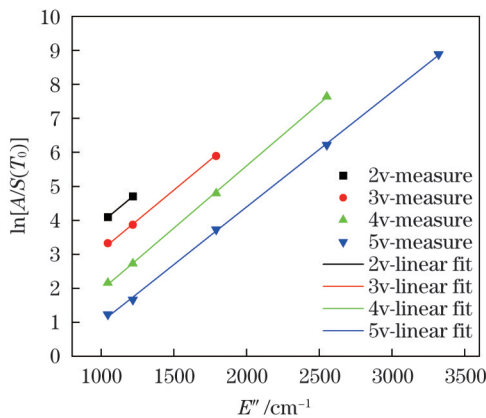


图 4 玻尔兹曼图法测温的拟合结果

Fig. 4 Fitting results of temperature measurement by Boltzmann diagram method

结果。

4.2 高温炉实验分析

对比了不同数目吸收线组合的测温精度,按照排列组合的方式,从 5 个波长中选择 2 组、3 组、4 组和 5 组波长进行计算,对应所选线组编号如表 2 所示。表 2 中将 7467.77、7444.36、7179.75、7185.597、6807.83 cm^{-1} 依次记为 ν_1 、 ν_2 、 ν_3 、 ν_4 、 ν_5 。

图 5 给出了不同谱线组合在 1000~1600 K 各温度段下计算的平均结果及标准差,分析可以得出以下结论:1) 双波长、三波长和四波长不同线组之间的测温结果不同,其中双波长不同谱线组合的测温精度差距较大,其主要原因是部分谱线的线强参数存在较大误差;随着波长数目增加,个别光谱参数误差的影响降低,三波长、四波长和五波长测温的精度增加,不同线

表 2 谱线组合方案
Table 2 Spectral line combination schemes

Number	Wavelength combination	Number	Wavelength combination
1	$\nu_1+\nu_2$	14	$\nu_1+\nu_3+\nu_4$
2	$\nu_1+\nu_3$	15	$\nu_1+\nu_3+\nu_5$
3	$\nu_1+\nu_4$	16	$\nu_1+\nu_4+\nu_5$
4	$\nu_1+\nu_5$	17	$\nu_2+\nu_3+\nu_4$
5	$\nu_2+\nu_3$	18	$\nu_2+\nu_3+\nu_5$
6	$\nu_2+\nu_4$	19	$\nu_2+\nu_4+\nu_5$
7	$\nu_2+\nu_5$	20	$\nu_3+\nu_4+\nu_5$
8	$\nu_3+\nu_4$	21	$\nu_1+\nu_2+\nu_3+\nu_4$
9	$\nu_3+\nu_5$	22	$\nu_1+\nu_2+\nu_3+\nu_5$
10	$\nu_4+\nu_5$	23	$\nu_1+\nu_3+\nu_4+\nu_5$
11	$\nu_1+\nu_2+\nu_3$	24	$\nu_2+\nu_3+\nu_4+\nu_5$
12	$\nu_1+\nu_2+\nu_4$	25	$\nu_1+\nu_2+\nu_3+\nu_4+\nu_5$
13	$\nu_1+\nu_2+\nu_5$		

组之间的偏差逐渐缩小。2) 在双波长及三波长测温中,低态能级相差较小的线对(如 $\nu_3+\nu_4$ 和 $\nu_2+\nu_3+\nu_4$) 在高温下不敏感,更容易受到光谱参数误差带来的影响,整体的温度测量值偏小,且变化平缓。3) 随着温度升高,各波长组合的测温精度降低,可能的原因是随着温度升高,恒温区内的控温精度下降,另外两端非测量区域少量残存的水汽通过热传递被加热至较高温度,对计算结果产生了影响。4) 五波长具有较高的测温精度,同时对光谱参数误差及环境误差的容忍度更大。

分别选取双波长(No.10)、三波长(No.19)、四波长(No.22)和五波长(No.25)中测温精度最高的线组与设定值进行对比,相对误差图如图 6 所示。可见,五波长与其他数目波长的测温结果相比,整体误差较小,且在所有温度下测量的相对误差均小于 1%。这一结果表明该测量方法对宽温度范围的测量具有较好的适应性,适用于发动机点火、升温、燃烧、降温、熄火全程的动态监测。

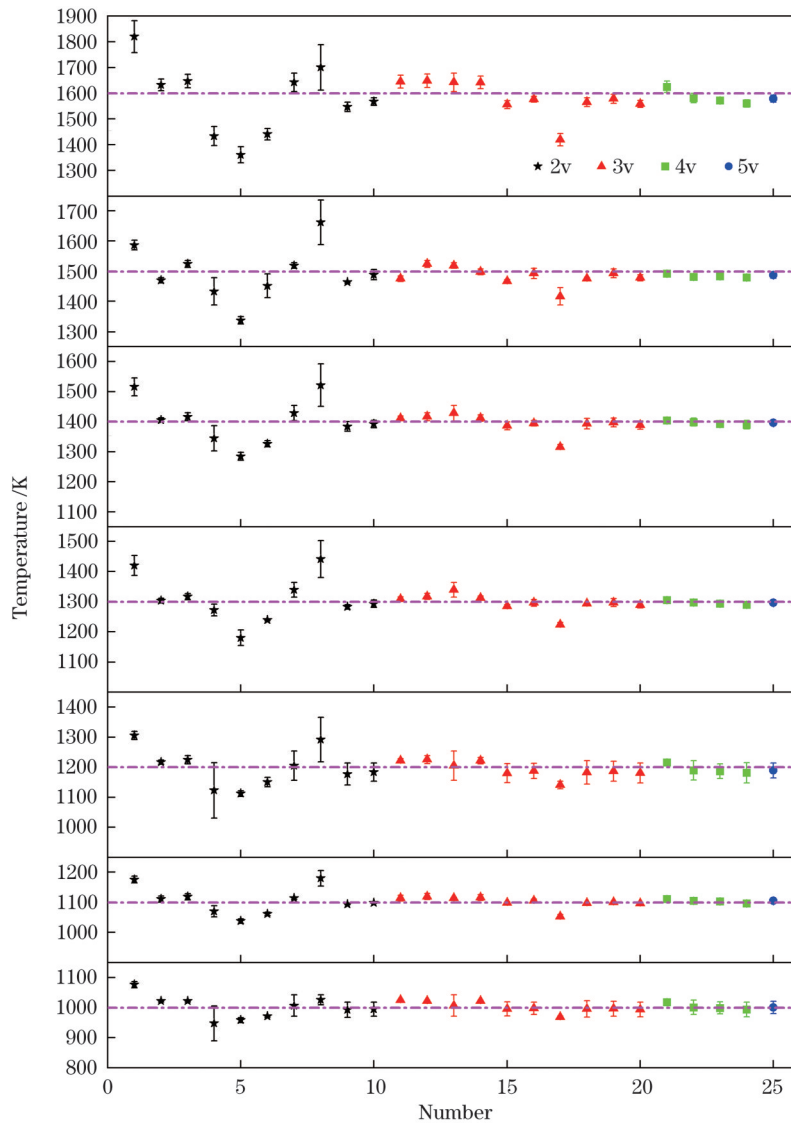


图 5 多波长组合测温结果

Fig. 5 Multi-wavelength combination temperature measurement results

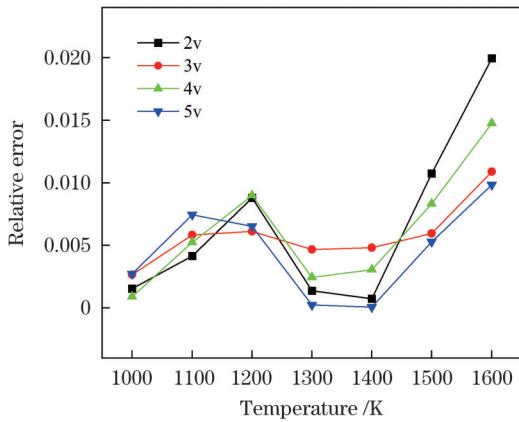


图 6 多波长测量相对误差对比

Fig. 6 Comparison of relative errors in multi-wavelength measurements

4.3 发动机扩张段实验

利用图 7 所示的直连式脉冲燃烧风洞设备开展温度测量实验。该风洞为脉冲吹吸式高超声速高温风洞,以航空煤油为燃料,可模拟飞行马赫数 4.0~7.0,总温为 900~1900 K,总压为 1.0~3.0 MPa,有效实验时长约为 0.5 s^[18]。实验开始前,将燃烧设备内部抽真空;实验开始后,注入冷空气,并注入氢气和氧气,点火加热空气,注入燃料点火。试验结束后关闭燃料、氢气和氧气,冷空气吹扫降温,最后关闭冷空气。

利用 TDLAS 测量扩张段温度,选取扩张段的某

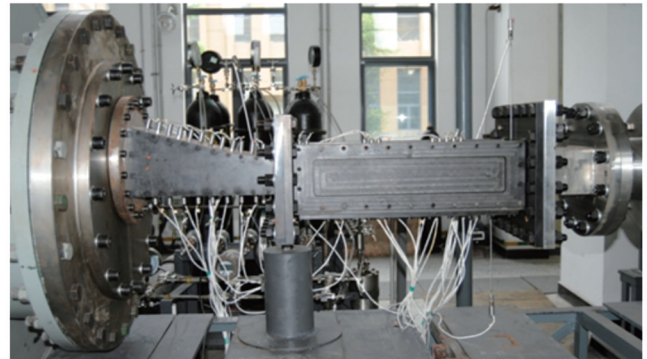
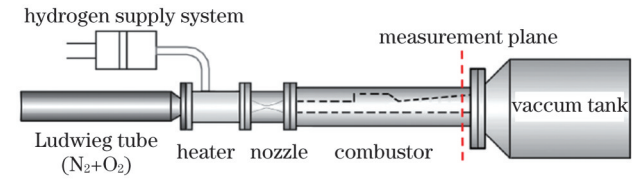


图 7 直连式脉冲燃烧风洞设备

Fig. 7 Direct-coupled pulsed combustion wind tunnel equipment

一横截面布置如图 8 所示的 11×5 光路,垂直方向布置 11 路,水平方向布置 5 路。采用实验室内集成的多波长 TDLAS 测量系统进行测量,系统出光后,输出光经分束器分成 16 束接入安装在扩张段壁面上的准直器,之后穿过内部待测流场,由另一端连接多模光纤的准直器收集,接着传输至信号探测与放大系统,并由采集卡采集。

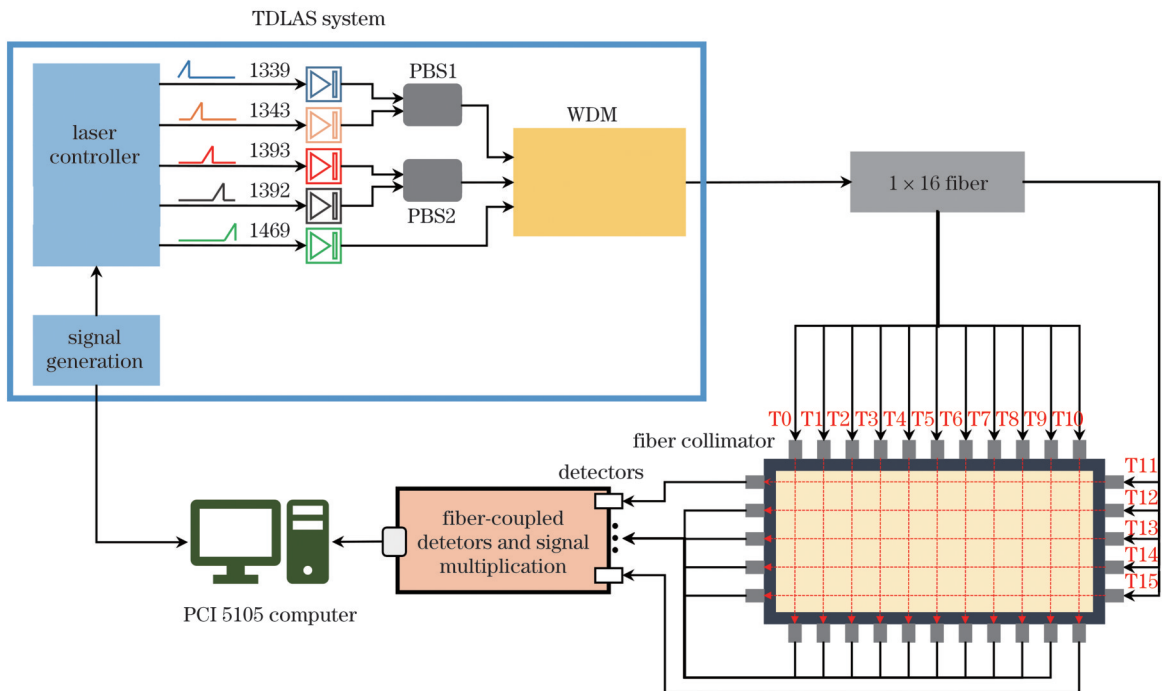


图 8 燃烧室扩张段测量方案

Fig. 8 Measurement scheme for the expansion section of the combustion chamber

4.4 发动机扩张段试验分析

进行若干工况下的发动机试验,选取工况 A 下的试验结果进行分析。对试验原始信号进行 20 次数据平均,

以提高数据的信噪比。1 s 内可获得 200 个点的有效数据。工况 A 下某一时刻的原始吸收信号如图 9 所示,其中 T0~T10 为垂直光路,T11~T15 为水平光路,该时刻

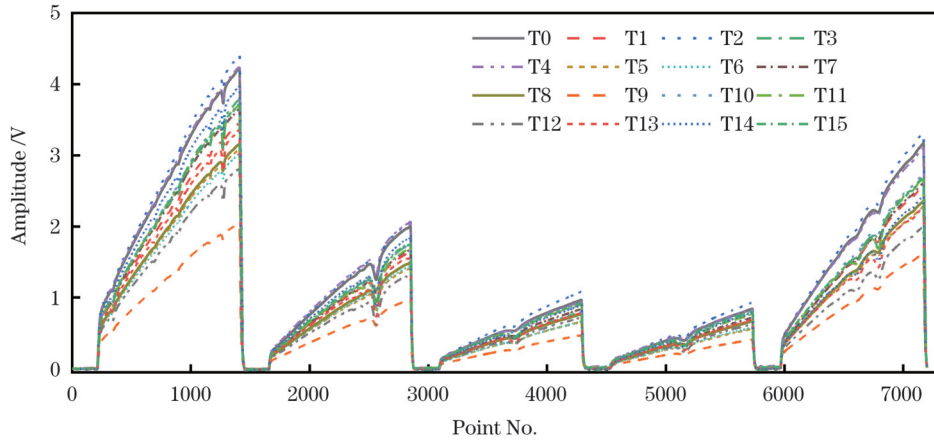


图 9 扩张段吸收信号

Fig. 9 Absorption signal of the expansion segment

下各光路信号无明显的畸变和抖动,信号质量较高。

图 10 和图 11 分别为工况 A 下垂直光路 T0~T10 和水平光路 T11~T15 的测量结果。0.2 s 时实验开始;约 0.2~0.4 s 内氢气点火,此时燃烧温度较低,垂直光路 T0~T10 呈两端温度高、中间温度低的分布趋势,而水平光路 T11~T15 温度依次降低(这是由于氢

气较轻,燃烧时浮于上方);0.4~0.9 s 为燃油点火阶段,温度陡增至约 1800 K;0.9 s 以后停止喷油,温度陡降后又缓慢降低,此时整体的温度分布依然呈现上高下低的趋势,这是冷却后热气流上升造成的。对比各光路的测温结果可以发现燃烧相对平稳,无明显的分布规律,高低温相差约 400 K。

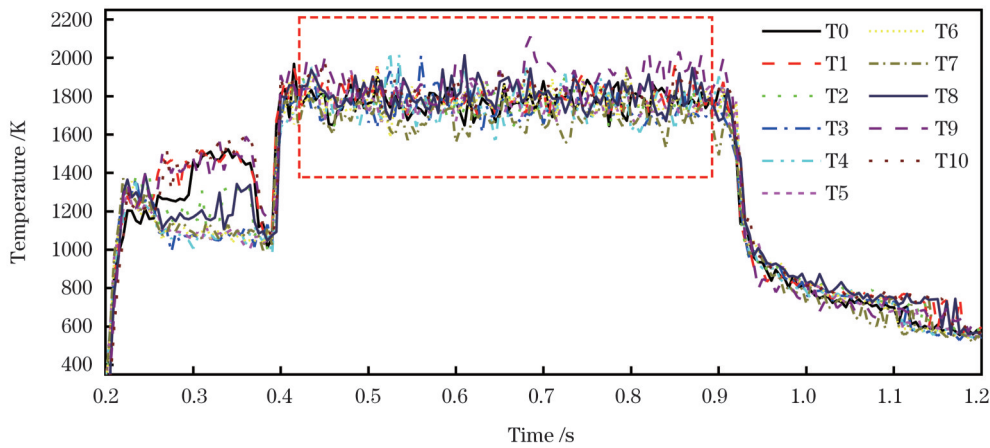


图 10 T0~T10 温度测量结果

Fig. 10 T0 - T10 temperature measurement results

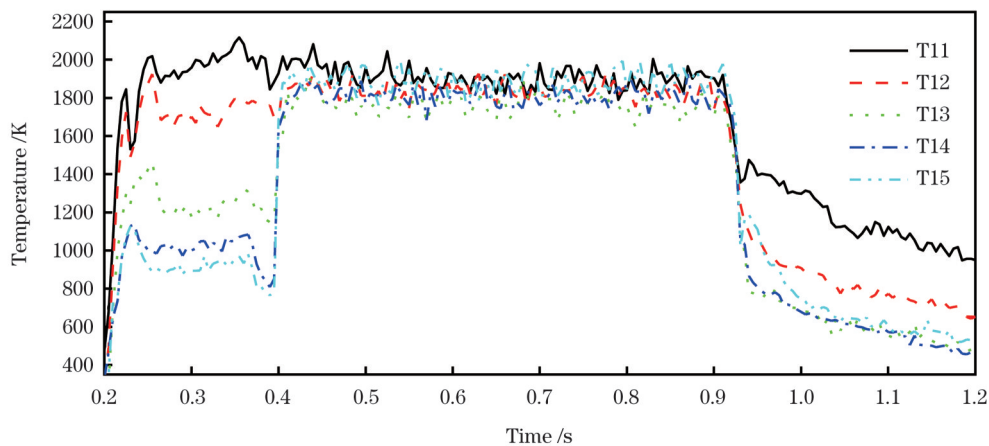


图 11 T11~T15 温度测量结果

Fig. 11 T11 - T15 temperature measurement results

对比工况 A(M6.5-033)和工况 B(M6.0-033)的两次重复实验,取燃油点火后的平稳段(如图 10 中红色虚线方框区域所示),计算各通道温度的平均值及标准偏差,计算结果如图 12 所示。在燃烧稳定段,工况 A 和工况 B 中 T11~T15 的温度分布均为上下高中间低,这与

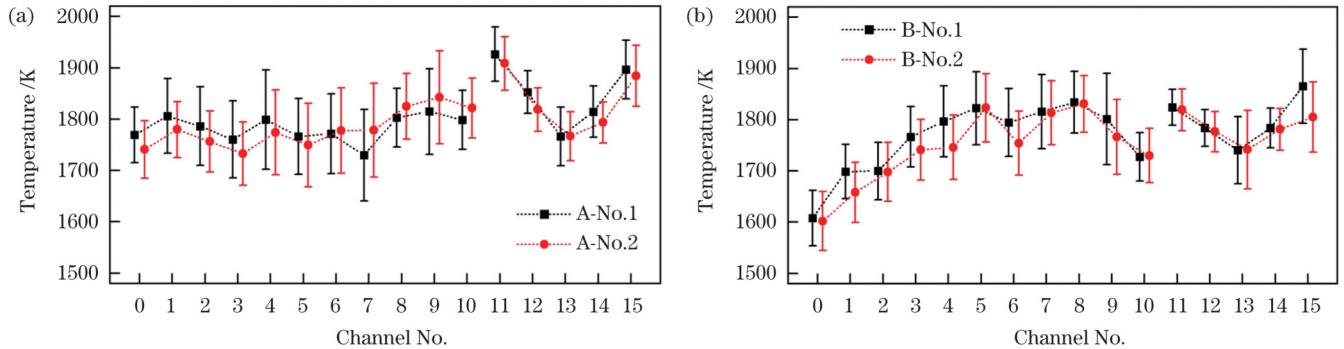


图 12 工况 A 和工况 B 下两次重复试验对比。(a) 工况 A; (b) 工况 B

Fig.12 Comparison of two repeated tests under condition A and condition B. (a) Condition A; (b) condition B

5 结 论

基于 TDLAS 技术,选取 5 个波长,采用玻尔兹曼图法进行温度测量。首先在实验室高温炉上进行了不同波长组合的温度测量实验,实验结果表明:随着波长数目增加,均匀温度场的测量结果受光谱参数及环境误差等的影响减小,测温精度提高,五波长的测温误差在 1% 以内,优于其他波长组合。五波长的温度测量结果在宽温度范围内均具有较高的精度,适合温度区间跨度大的燃烧环境。此外,在超燃冲压发动机扩张段测量了 16 个光路的平均温度,对比相同工况下的两次试验结果,结果显示:测量结果具有较高的一致性,两个工况下重复试验的平均偏差分别为 17 K 和 7 K,验证了该测量方法的稳定性。该方法可在燃烧剧烈的发动机燃烧流场下获得良好的测量结果。后续拟为燃烧截面的场分布重建提供更多的波长信息,以提高场分布重建的精度。

参 考 文 献

- [1] 阚瑞峰, 夏晖晖, 许振宇, 等. 激光吸收光谱流场诊断技术应用研究与进展[J]. 中国激光, 2018, 45(9): 0911005.
Kan R F, Xia H H, Xu Z Y, et al. Research and progress of flow field diagnosis based on laser absorption spectroscopy[J]. Chinese Journal of Lasers, 2018, 45(9): 0911005.
- [2] 聂伟, 阚瑞峰, 杨晨光, 等. 可调谐二极管激光吸收光谱技术的应用研究进展[J]. 中国激光, 2018, 45(9): 0911001.
Nie W, Kan R F, Yang C G, et al. Research progress on the application of tunable diode laser absorption spectroscopy[J]. Chinese Journal of Lasers, 2018, 45(9): 0911001.
- [3] Goldenstein C S, Spearin R M, Jeffries J B, et al. Infrared laser-absorption sensing for combustion gases[J]. Progress in Energy and Combustion Science, 2017, 60: 132-176.
- [4] 张光乐. 基于多吸收线 TDLAS 的一维温度不均匀性测量方法研究[D]. 北京: 中国科学院大学, 2016: 20-23.
Zhang G L. Research on one-dimensional temperature inhomogeneity measurement method based on multi-absorption line TDLAS[D]. Beijing: University of Chinese Academy of Sciences, 2016: 20-23.
- [5] Li Y, Wang S K, Strand C L, et al. Development of a Stark shift measurement technique using excited-state oxygen atoms to determine electron number density in shock heated O₂/Ar above 10000 K[J]. Plasma Sources Science and Technology, 2021, 30(2): 025007.
- [6] 许振宇, 刘文清, 刘建国, 等. 基于可调谐半导体激光器吸收光谱的温度测量方法研究[J]. 物理学报, 2012, 61(23): 234204.
Xu Z Y, Liu W Q, Liu J G, et al. Temperature measurements based on tunable diode laser absorption spectroscopy[J]. Acta Physica Sinica, 2012, 61(23): 234204.
- [7] Tancin R J, Goldenstein C S. Ultrafast-laser-absorption spectroscopy in the mid-infrared for single-shot, calibration-free temperature and species measurements in low- and high-pressure combustion gases[J]. Optics Express, 2021, 29(19): 30140-30154.
- [8] Gordon I E, Rothman L S, Hargreaves R J, et al. The HITRAN2016 molecular spectroscopic database[J]. Journal of Quantitative Spectroscopy and Radiative Transfer, 2017, 203: 3-69.
- [9] 杨文斌, 齐新华, 王林森, 等. 基于 CARS 技术的超燃冲压发动机点火过程温度测量[J]. 气体物理, 2020, 5(2): 8-13.
Yang W B, Qi X H, Wang L S, et al. Temperature measurement based on CARS in scramjet ignition process[J]. Physics of Gases, 2020, 5(2): 8-13.
- [10] Wang Z Z, Zhou W Z, Kamimoto T, et al. Two-dimensional temperature measurement in a high-temperature and high-pressure combustor using computed tomography tunable diode laser absorption spectroscopy (CT-TDLAS) with a wide-scanning laser at 1335-1375 nm[J]. Applied Spectroscopy, 2020, 74(2): 210-222.
- [11] 艾苏曼, 邓昊, 黄安, 等. 基于宽波段吸收光谱测温方法的影响因素数值研究[J]. 光学学报, 2022, 42(18): 1830003.
Ai S M, Deng H, Huang A, et al. Numerical study on influencing factors of thermometry method based on broadband absorption spectra[J]. Acta Optica Sinica, 2022, 42(18): 1830003.
- [12] 司赶上, 刘家祥, 李振钢, 等. 基于形态学与多项式拟合的紫外拉曼荧光背景扣除算法[J]. 光学学报, 2022, 42(22): 2230001.
Si G S, Liu J X, Li Z G, et al. Fluorescence background subtraction algorithm of UV raman based on morphology and polynomial fitting[J]. Acta Optica Sinica, 2022, 42(22): 2230001.
- [13] Busa K M, Brown M S, Gruber M, et al. Common-path measurement of H₂O, CO, and CO₂ via TDLAS for combustion progress in a hydrocarbon-fueled scramjet[C]//54th AIAA Aerospace Sciences Meeting, January 4-8, 2016, San Diego,

- California, USA. Virginia: AIAA Press, 2016: 0659.
- [14] Goldenstein C S, Spearrin R M, Schultz I A, et al. Wavelength-modulation spectroscopy near 1.4 μm for measurements of H_2O and temperature in high-pressure and-temperature gases[J]. Measurement Science and Technology, 2014, 25(5): 055101.
- [15] 张乐文, 孙鹏帅, 刘旭, 等. 基于单一量子级联激光器的大气多组分气体(CO 、 N_2O 、 H_2O)同时测量方法[J]. 光学学报, 2022, 42(4): 0430002.
- Zhang L W, Sun P S, Liu X, et al. Simultaneous measurement of atmospheric multi-component (CO , N_2O , and H_2O) based on single quantum cascaded laser[J]. Acta Optica Sinica, 2022, 42(4): 0430002.
- [16] Jacob J F. High temperature and pressure measurements from TDLAS through the application of 2nd derivative fitting and the aggregate Boltzmann method[D]. Ann Arbor: The University of Michigan, 2019: 22-24.
- [17] 陈玖英, 周梅, 刘建国, 等. CO_2 高温光谱参数测量系统设计与实验[J]. 红外与毫米波学报, 2019, 38(3): 358-364.
- Chen J Y, Zhou M, Liu J G, et al. Design and experiment of CO_2 high temperature spectrum parameter measurement system[J]. Journal of Infrared and Millimeter Waves, 2019, 38(3): 358-364.
- [18] 杨文斌, 齐新华, 李猛, 等. 超燃冲压发动机燃烧室出口温度场分布 CARS 测量[J]. 推进技术, 2022, 43(9): 364-371.
- Yang W B, Qi X H, Li M, et al. Outlet temperature measurements of scramjet combustor using coherent anti-stokes Raman scattering [J]. Journal of Propulsion Technology, 2022, 43(9): 364-371.

Temperature-Measurement Method Based on Boltzmann Diagram for Scramjet Engine

Huang An^{1,2}, Zhao Yanhui³, Yang Shunhua³, Xia Huihui¹, Deng Hao¹, Ruan Jun¹, Hu Jiayi¹,
Ai Suman¹, Xu Zhenyu^{1*}, Kan Ruifeng^{1**}

¹Anhui Institute of Optics and Fine Mechanics, Hefei Institutes of Physical Science, Chinese Academy of Sciences,
Hefei 230031, Anhui, China;

²Science Island Branch, Graduate School of University of Science and Technology of China, Hefei 230026, Anhui, China;

³Hypervelocity Aerodynamics Institute, China Aerodynamics Research and Development Center, Mianyang
621000, Sichuan, China

Abstract

Objective Tunable diode laser absorption spectroscopy (TDLAS) is a powerful technology to measure the temperature of burners, such as industrial boilers, scramjet engines, gas turbines, and aero engines. Currently, in TDLAS-based thermometers, two-line thermometry is a common method for calculating the temperature of the target devices based on the monotone variation relation between the ratio of two selected absorption linestrengths and the corresponding temperature. However, the range and accuracy of temperature measurements strongly depend on the absorption linestrengths and the corresponding low-energy levels. Thus, improper selection of the two absorption lines may limit the temperature-measurement range and induce a significant measurement error. In addition, the error is influenced by the uncertainty of the line parameters. Recently, a multiline temperature-measurement method has been developed to improve the tolerance of the measurement error induced by the uncertainty of the line parameters, which can be achieved by scanning with an external cavity laser (ECL) with a wide wavelength region to cover several more absorption lines. However, using ECL may result in problems, such as the difficult baseline retrieval caused by the irregular variation of the emission intensity in the wavelength scanning region and the low temporal resolution limited by the response speed of the ECL internal mechanical motor.

Methods Considering the above ECL limitations, a multiple distributed feedback (DFB) laser-based TDLAS system was developed to measure water vapor (H_2O) absorption lines near 1339, 1343, 1392, 1393, and 1469 nm. The wavelengths of the lasers can be tuned to match the absorption region of interest by adjusting the lasers' temperatures and injection currents with homemade laser temperature and current controllers. Five time-division multiplexing ramp signals were generated using an FPGA-based function generator to control the injection currents of the laser. The laser beams were collimated and passed through the gas medium in tube furnaces and scramjet engines. The transmitted beams were collected on photodetectors, and the corresponding H_2O absorptions were recorded using an FPGA-based data acquisition circuit. In this study, we applied a typical multiline temperature-measurement method using Boltzmann diagrams to calculate the temperature of the target species. Temperatures ranging from 1000 K to 1600 K were measured in the high-temperature tube furnace (Fig. 2) to assess the performance of this system. Subsequently, the cross-sectional temperatures of the expansion section of the scramjet engine were measured (Fig. 8), where 16 optical paths were arranged in the wall openings of the expansion section. Two experiments were performed under the same conditions to verify the repeatability of the experiment.

Results and Discussions The high-temperature tube furnace measurements show that the temperature-measurement accuracy, as expected, presents a strong dependency on the number of the selected absorption lines (Fig. 5) and is enhanced by increasing the absorption lines. A relative measurement error of less than 1% for the temperature range of 1000–1600 K can be achieved by using five H_2O absorption lines; this error is lower than that induced by using a smaller number of absorption lines, indicating that the five

wavelengths have good adaptability to the measurement over a wide temperature range (Fig. 6). For the scramjet, the measured hydrogen combustion time and fuel combustion time are approximately 0.2 and 0.5 s, respectively. Moreover, the experimental results show that hydrogen combustion is distributed in the upper layer of the expansion section before and after fuel ignition, and the combustion state remains stable owing to the small temperature difference between the set optical paths when the fuel is burned. To test the repeatability of the hydrogen combustion state, we repeated the same experiment twice for the preset conditions A and B. The final results indicate that the two experiments for the same condition have good repeatability, where the average deviation of the temperature measurement is approximately 16 K for the two experiments under condition A, whereas the average temperature is approximately 7 K for the two experiments under condition B.

Conclusions In this study, we have developed a miniaturized TDLAS system using multiple DFB lasers as light sources to measure the temperatures of H_2O in a high-temperature tube furnace and scramjet. A Boltzmann diagram-based multiline temperature-measurement approach is used to improve temperature-measurement precision. The temperature-measurement performance of the furnace using different numbers of H_2O absorption lines is assessed in terms of the measurement error, and the optimized number of H_2O absorption lines is determined to be five. A temperature measurement error of 1% is obtained by using five H_2O absorption lines to calculate the temperature, which also illustrates that the method used in this study is suitable for temperature measurement with a wide temperature range and high accuracy for complex combustion environments. In addition, the linear average temperature is measured in the expansion section of the scramjet engine at different positions of the cross-section, and the experimental results show that the hydrogen combustion state remains highly consistent according to the average deviations of the two experiments of temperature measurement for different preset conditions A and B. All the above results indicate that the current method based on the Boltzmann diagram shows a high potential for high-precision temperature measurements in the combustion flow field, such as in engines with intense combustion. This method will be further developed to provide more wavelength information for the field distribution reconstruction of combustion and improve accuracy.

Key words spectroscopy; tunable diode laser absorption spectroscopy; Boltzmann diagram; temperature measurement